

A Simple Generic Model of Cellular Polarity Alignment: Derivation and Analysis

Kaori Sugimura¹ and Hiroshi Kori^{1,*}

¹*Department of Information Sciences, Ochanomizu University, Tokyo 112-8610, Japan*
(Dated: December 19, 2021)

Ordered polarity alignment of a cell population plays a vital role in biology, such as in hair follicle alignment and asymmetric cell division. Here, we propose a theoretical framework for the understanding of generic dynamical properties of polarity alignment in interacting cellular units, where each cell is described by a reaction-diffusion system and the cells further interact with one another through their proximal surfaces. The system behavior is shown to be strongly dependent on geometric properties such as cell alignment and cell shape. Using a perturbative method under the assumption of weak coupling between cells, we derive a reduced model in which each cell is described by just one variable, the phase. The reduced model resembles an XY model but contains novel terms that possesses geometric information, which enables the understanding of the geometric dependencies as well as the effects of external signal and noise. The model is simple, generic, and analytically and numerically tractable, and is therefore expected to facilitates studies on cellular polarity alignment in various nonequilibrium systems.

PACS numbers: 05.45.-a, 82.40.Ck, 87.18.Hf

Introduction–. Spatially ordered patterns are ubiquitous in nature and have been of central importance in various disciplines [1–3]. This work is concerned with dynamical alignment of polarity in interacting cellular units. Spin is a prototypical example of a polar unit. Spins are spatially aligned to magnetize through spin-spin interaction and their response to an external field, as described by, e.g., Ising and XY models [4]. The present work focuses on nonequilibrium systems, including chemical and biological systems. Polarity can be regarded as an asymmetric distributions in chemical species within a cellular unit. Polarity is of great importance in biology because it is essential for, e.g., cell movement and oriented cell division [5]. Moreover, cell polarity is often spatially coordinated across a cell population for functional reasons. A well-known example in biology is planar cell polarity (PCP), which refers to the coordinated alignment of cell polarity across planar tissue. This underlies the alignment of, e.g., hair follicles and cilia positioning [5]. So far, several mathematical models have been proposed to address the effects of various factors on polarity alignment including cell shape, external signal, and noise. Some studies employ detailed models, where each cell is described by a reaction-diffusion system and these cells are further coupled through proximal membranes [6, 7]. Some studies employ simple phenomenological models similar to models for magnetization [8, 9], which is a reasonable approach because the cell alignment process phenomenologically resembles magnetization. The former contains many free parameters and is too complicated to provide general understandings. On the other hand, in the latter, models are rather arbitrary and may lack essential dynamical features.

In the present Letter, the generic dynamical properties of cell polarity alignment are examined, through deriving a reduced model for coupled reaction-diffusion systems using a perturbative method. In our reaction-diffusion model, each cell is described by a reaction-diffusion system and the cells mutually inhibit one another through their proximal surfaces. Its reduced model, referred to as a phase model, is drastically simple yet reasonably approximates the original reaction-diffusion model when cells are weakly coupled. Our phase model resembles the XY model but includes novel terms representing geometric information such as cell shape and the relative position between neighboring cells. By taking advantage of its tractability, essential dynamical properties including the effects of cell shape, external signal, and noise are analytically clarified, which has only been studied numerically in previous studies using detailed models [6–8]. Our study bridges the gap between detailed and phenomenological models, and is expected to facilitate the study of polarity dynamics in various nonequilibrium systems.

Model–. Our entire system is composed of a population of cells aligned in two-dimensional space. Reaction-diffusion dynamics of each cell take place on the one-dimensional surface of their perimeter 2π , and the cells further interact with one another through the proximal surfaces between them. Each cell obeys

$$\frac{\partial}{\partial t} \mathbf{X}_i = \mathbf{F}(\mathbf{X}_i) + \hat{D} \frac{\partial^2 \mathbf{X}_i}{\partial \theta_i^2} + \epsilon \sum_{j \in A(i)} \mathbf{H}_{ij}, \quad (1)$$

where $\mathbf{X}_i = \mathbf{X}_i(\theta_i, t)$ ($i = 1, \dots, N$) denotes the concentration of chemical species at time t and the position θ_i ($0 \leq \theta_i < 2\pi$) on the surface of each cell, \mathbf{F} describes the local reaction dynamics, \hat{D} is the diagonal matrix consisting of diffusion coefficients, $A(i)$ is the set of cells adjacent to cell i , \mathbf{H}_{ij} describes intercellular interaction, and ϵ is the coupling strength. As will be described later, external

* corresponding author: kori.hiroshi@is.ocha.ac.jp

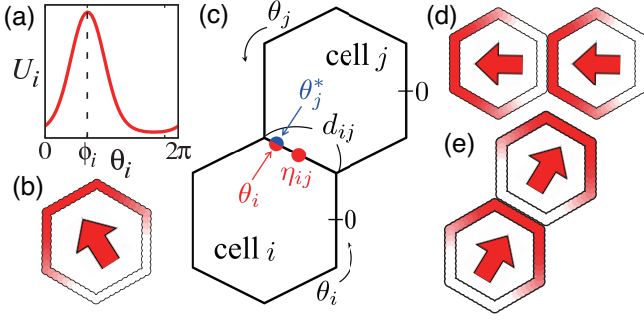


FIG. 1. (Color online). (a) Unimodal distribution on the surface of a cell and polarity orientation. (b) Color scale representation and polarity orientation corresponding to (a). (c) Model description. (d,e) Examples of polarity patterns of two coupled cells with different cell alignments.

signal and noise may also be considered. Note that \mathbf{H}_{ij} is generally a functional of $\mathbf{X}_i(\theta_i, \cdot)$ and $\mathbf{X}_j(\theta_j, \cdot)$. Each cell is assumed to exhibit a unimodal distribution for $\varepsilon = 0$; i.e., polarity is spontaneously formed. The polarity orientation of cell i is defined by the θ_i value at which the first component of $\mathbf{X}_i(\theta_i, t)$, denoted by $U_i(\theta_i, t)$, takes its maximum [see Figs. 1(a,b)].

As examples, we consider two models: (a) the real Ginzburg-Landau equation (GLE) and (b) the activator-inhibitor model. Both of these models have two variables, denoted by $\mathbf{X}_i = (U_i, V_i)$ (see Supplemental Material A for details). The former is a long-wave amplitude equation, which is widely used to describe various systems near the onset of instability. The latter is a reaction-diffusion model, describing biological pattern formation [10]. In these models, given appropriate initial conditions, \mathbf{X}_i exhibits a stationary unimodal distribution within individual cells for $\varepsilon = 0$, thus they are suitable as dynamical models describing cell polarity.

Intercellular interaction is assumed to occur at every contact point of the neighboring cells. Geometric parameters are defined as shown in Fig. 1(c), where η_{ij} and d_{ij} are the midpoint and the length of the proximal surface between cell i and j , respectively, and θ_j^* is the position in cell j facing θ_i in cell i . The interaction function is given as

$$\mathbf{H}_{ij} = (S_{ij}(\theta_i - \eta_{ij}) \{U_i(\theta_i) - U_j(\theta_j^*)\}, 0). \quad (2)$$

where $S_{ij}(\theta_i - \eta_{ij})$ describes the position of contact, given as $S_{ij}(\theta) = 1$ for $|\theta| \leq \frac{d_{ij}}{2}$ and $S_{ij}(\theta) = 0$ otherwise. When the cell has a regular hexagonal shape, which is assumed henceforth unless otherwise noted, we have $d_{ij} = \frac{\pi}{3}$ and $\theta_j^* = \pi + 2\eta_{ij} - \theta_j$. The latter relationship holds true also for elongated hexagonal shapes introduced later. For $\varepsilon > 0$, Eq. (2) describes mutual inhibition of U component between proximal cells. With this interaction, the polarities of two neighboring cells are expected to align along their relative position of the cells, i.e., η_{ij} or $\pi + \eta_{ij}$, because the surface of cell i with high U tends to face that of cell j with low U , as is illustrated in Figs. 1(d)

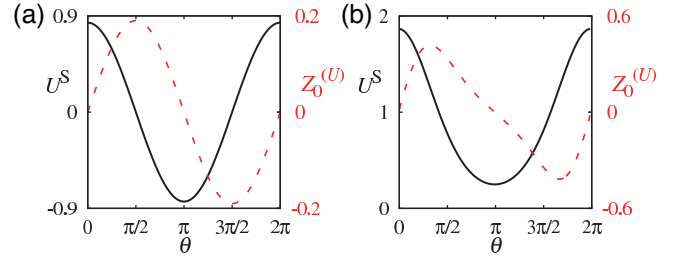


FIG. 2. (Color online). The profile of the steady state $U^S(\theta)$ (solid lines) and the phase sensitivity function $Z_0^{(U)}(\theta)$ (dashed lines) for (a) the GLE and (b) the activator-inhibitor model.

and (e).

Derivation of the phase model-. We derive a reduced model for Eq. (1) using a perturbative method. Our method is based on well-known phase reduction theory [11] and is an application of the recently developed method for oscillatory patterns reported in Refs. [12, 13].

Let $\mathbf{X}^S(\theta)$ be the stationary distribution of a cell in the unperturbed system ($\varepsilon = 0$). Because of the translational symmetry, $\mathbf{X}^S(\theta - \theta_0)$ with any constant θ_0 is also a steady solution. The phase $\phi_i(t)$ of the $\mathbf{X}_i(\theta_i, t)$ is defined such that $\mathbf{X}_i(\theta_i, t)$ converges to $\mathbf{X}^S(\theta_i - \phi)$ as $t \rightarrow \infty$ in the unperturbed system. In other words, $\mathbf{y}_i(\theta_i, t) \rightarrow 0$ as $t \rightarrow \infty$ for $\varepsilon = 0$, where the deviation $\mathbf{y}_i(\theta_i, t)$ is defined by

$$\mathbf{X}_i(\theta_i, t) = \mathbf{X}^S(\theta_i - \phi_i) + \mathbf{y}_i(\theta_i, t), \quad (3)$$

with ϕ_i being the phase of the state $\mathbf{X}_i(\theta_i, t)$. Without loss of generality, we assume that $U^S(\theta)$, which is the U component of $\mathbf{X}^S(\theta)$, takes its maximum at $\theta = 0$. Then, for sufficiently small $\mathbf{y}_i(\theta_i, t)$, $\phi_i(t)$ of $\mathbf{X}_i(\theta_i, t)$ is well approximated by the maximum of $U_i(\theta_i, t)$, i.e.,

$$\phi_i(t) \approx \arg\max_{\theta_i} U_i(\theta_i, t). \quad (4)$$

Thus, ϕ_i may be regarded as the polarity orientation of cell i .

The linear operator \mathcal{L} is defined by $\mathcal{L} = J + \hat{D} \frac{\partial^2}{\partial \theta^2}$ with Jacobian $J = \partial \mathbf{F}(\mathbf{X}) / \partial \mathbf{X}$ estimated at $\mathbf{X} = \mathbf{X}^S(\theta)$. The adjoint operator \mathcal{L}^\dagger is defined such that it satisfies $\langle \mathbf{A}, \mathcal{L} \mathbf{B} \rangle = \langle \mathcal{L}^\dagger \mathbf{A}, \mathbf{B} \rangle$, where the inner product of the 2π -periodic functions, $\mathbf{A}(\theta)$ and $\mathbf{B}(\theta)$, is defined by $\langle \mathbf{A}, \mathbf{B} \rangle = \int_0^{2\pi} \mathbf{A} \cdot \mathbf{B} d\theta$. For our model (1), we can show that $\mathcal{L}^\dagger = J^T + \hat{D} \frac{\partial^2}{\partial \theta^2}$, where J^T is the transpose of J . The eigenfunctions of \mathcal{L} and \mathcal{L}^\dagger are denoted by $\mathbf{Y}_\ell(\theta)$ and $\mathbf{Z}_\ell(\theta)$ ($\ell = 0, 1, \dots$), respectively. In particular, the zero-eigenfunctions are denoted by \mathbf{Y}_0 and \mathbf{Z}_0 , i.e., $\mathcal{L} \mathbf{Y}_0 = \mathcal{L}^\dagger \mathbf{Z}_0 = 0$. Here, we choose $\mathbf{Y}_0 = -\frac{\partial \mathbf{X}^S}{\partial \theta}$. These eigenfunctions are assumed to form a complete orthonormal system and are normalized as $\langle \mathbf{Z}_\ell, \mathbf{Y}_m \rangle = \delta_{\ell m}$. The deviation \mathbf{y}_i can be expanded as

$$\mathbf{y}_i(\theta_i, t) = \sum_{\ell=1}^{\infty} C_\ell(t) \mathbf{Y}_\ell(\theta_i - \phi_i), \quad (5)$$

where ϕ_i is the phase of the state $\mathbf{X}_i(\theta_i, t)$. Note that $\mathbf{Y}_0(\theta_i - \phi_i)$ is absent in this expansion because $\mathbf{y}_i(\theta_i, t) \rightarrow 0$ as $t \rightarrow \infty$ for $\varepsilon = 0$.

Substituting Eq. (3) into Eq. (1), we obtain

$$\mathbf{Y}_0(\theta_i - \phi_i)\dot{\phi}_i + \dot{\mathbf{y}}_i = \mathcal{L}\mathbf{y}_i + \varepsilon \sum_{j \in A(i)} \mathbf{H}_{ij} + O(\varepsilon^2). \quad (6)$$

Taking the inner product with $\mathbf{Z}_0(\theta_i - \phi_i)$ and dropping $O(\varepsilon^2)$, we finally obtain the phase model given as

$$\dot{\phi}_i = \varepsilon \sum_{j \in A(i)} \Gamma_{ij}(\phi_i, \phi_j), \quad (7)$$

$$\Gamma_{ij} = \langle \mathbf{Z}_0(\theta_i - \phi_i), \mathbf{H}_{ij}^S \rangle, \quad (8)$$

where $\mathbf{H}_{ij}^S = \mathbf{H}_{ij} \{ \mathbf{X}^S(\theta_i - \phi_i), \mathbf{X}^S(\theta_j - \phi_j) \}$. Given the functional forms of $\mathbf{X}^S(\theta)$ and $\mathbf{Z}_0(\theta)$, Eq. (7) provides a closed equation for the phases ϕ_i ($i = 1, \dots, N$).

It is convenient to express Γ_{ij} in terms of the Fourier coefficients defined by $U^S(\theta) = \sum_{k=-\infty}^{\infty} u_k \cos k\theta$, $Z_0^{(U)}(\theta) = \sum_{k=-\infty}^{\infty} -z_k \sin k\theta$, and $S_{ij}(\theta) = \sum_{k=-\infty}^{\infty} s_k^{(ij)} \cos k\theta$ ($u_k, z_k, s_k \in \mathbb{R}$), where we assumed that $S_{ij}(\theta)$, $U^S(\theta)$, and $Z_0^{(U)}(\theta)$ are even, even, and odd functions, respectively. Substitute these expansions into Eq. (8) with \mathbf{H}_{ij} given by Eq. (2), we obtain a general expression:

$$\Gamma_{ij} = 2\pi \sum_{k,l} z_k u_l \left[(-1)^l s_{l-k}^{(ij)} \sin \{ (k+l)\eta_{ij} - k\phi_i - l\phi_j \} - s_{-k-l}^{(ij)} \sin \{ (k+l)(\eta_{ij} - \phi_i) \} \right]. \quad (9)$$

For a regular hexagonal cell shape, we have $s_k^{(ij)} = \frac{1}{k\pi} \sin \frac{k d_{ij}}{2}$ ($k \neq 0$), $s_0^{(ij)} = \frac{d_{ij}}{2\pi}$. The coefficients u_k and z_k are obtained for a given model.

For the GLE, the phase reduction is analytically performed. By solving $\mathbf{F}(\mathbf{X}^S) + \hat{D} \frac{\partial^2}{\partial \theta^2} \mathbf{X}^S = 0$, we obtain $\mathbf{X}^S = (U^S, V^S) = \sqrt{1-D_0}(\cos \theta, \sin \theta)$. By solving $\mathcal{L}^\dagger \mathbf{Z}_0 = 0$ with the normalization $\langle \mathbf{Z}_0, \mathbf{Y}_0 \rangle = 1$, where $\mathcal{L}^\dagger = \mathcal{L}$ in the present model, we obtain $\mathbf{Z}_0 = (Z_0^{(U)}, Z_0^{(V)}) = \frac{1}{2\pi\sqrt{1-D_0}}(\sin \theta, -\cos \theta)$ [Fig. 2(a)]. Therefore, Eq. (9) reduces to

$$\Gamma_{ij}(\phi_i, \phi_j) = a_{ij} \sin(\phi_j - \phi_i) + a_{ij} \sin 2(\eta_{ij} - \phi_i) + b_{ij} \sin(2\eta_{ij} - \phi_i - \phi_j) \quad (10)$$

with $a_{ij} = \frac{\sin d_{ij}}{4\pi}$ and $b_{ij} = \frac{d_{ij}}{4\pi}$. For general models, phase reduction is performed numerically by solving Eq. (1) for $\varepsilon = 0$ and its adjoint equation $\dot{\mathbf{Z}}_0 = \mathcal{L}^\dagger \mathbf{Z}_0$ with $\langle \mathbf{Z}_0, \mathbf{Y}_0 \rangle = 1$ [13]. For the activator-inhibitor model, U^S and $Z_0^{(U)}$ are obtained, as shown in Fig. 2(b). Their Fourier coefficients are approximately given as $u_0 = 0.925, u_1 = 0.397, u_2 = 0.065, z_1 = -0.180$, and $z_2 = -0.062$. Other coefficients are negligible in this case. For both the GLE and the activator-inhibitor models, the accuracy of our reduction theory is confirmed by

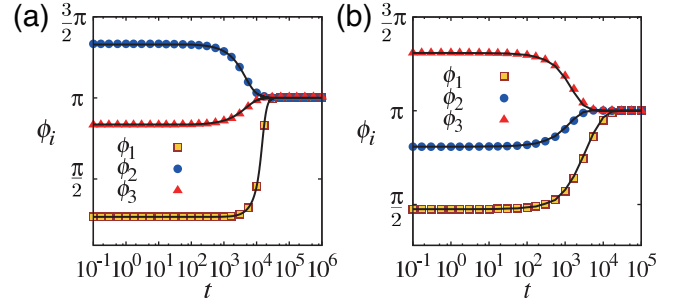


FIG. 3. (Color online). Comparison between the time series obtained from the reaction-diffusion models (symbols) and the corresponding phase models (lines). (a) GLE. (b) Activator-inhibitor model. In this case, three hexagonal cells are aligned in a row, i.e., $\eta_{12} = \eta_{23} = 0, d_{12} = d_{23} = \frac{\pi}{3}$.

comparing the time series of the original model given by Eq. (1) and that of the phase model given by Eqs. (7) and (10), with the corresponding Γ_{ij} , as shown in Fig. 3.

It should be noted that the phase sensitivity function $\mathbf{Z}_0(\theta)$ is very useful for understanding the response of the polarity orientation to perturbation. See Fig. 2(a) as an example. If the U variable is perturbed upward at $\theta = \pi/2$, ϕ will increase because $\mathbf{Z}_0(\pi/2) > 0$, i.e., the pattern will eventually shift right.

Analysis. We focus on the phase model with Eq. (10) below because of the following reason. If $U^S(\theta)$ and $Z_0^{(U)}(\theta)$ are nearly harmonic, i.e., u_k and z_k ($k \geq 2$) are small, we approximately obtain $\Gamma_{ij} = -4\pi z_1 u_1 [s_2^{(ij)} \sin(\phi_j - \phi_i) + s_2^{(ij)} \sin 2(\eta_{ij} - \phi_i) + s_0^{(ij)} \sin(2\eta_{ij} - \phi_i - \phi_j)]$, which is Eq. (10) with generally different coefficients. Therefore, the coupling function given by Eq. (10) is of crucial importance.

We first consider two coupled cells with $\eta_{12} = 0, \eta_{21} = \pi, a_{12} = a_{21}, b_{12} = b_{21}$, and investigate the existence and stability of the in-phase state. Substituting the in-phase state $(\phi_1, \phi_2) = (\phi^*, \phi^*)$ into Eq. (7) with Eq. (10), we obtain $\sin 2\phi^* = 0$, thus $\phi^* = 0, \pi$ or $\phi^* = \pm \frac{\pi}{2}$. Putting $\phi_i = \phi^* + \psi_i$ ($i = 1, 2$), $\xi = \psi_1 + \psi_2$ and $\zeta = \psi_1 - \psi_2$, and linearizing Eq. (7) for small ψ_i , we obtain

$$\dot{\xi} = -2\epsilon(a_{ij} + b_{ij})(\cos 2\phi^*)\xi \quad (11)$$

$$\dot{\zeta} = -2\epsilon a_{ij}(1 + \cos 2\phi^*)\zeta. \quad (12)$$

The solutions $(0, 0)$ and (π, π) are thus linearly stable when $\epsilon a_{ij} > 0$ and $\epsilon(a_{ij} + b_{ij}) > 0$. The GLE with $\epsilon > 0$ satisfies this condition. In contrast, the solution $\phi = \pm \frac{\pi}{2}$ may not be asymptotically stable because $\dot{\zeta}$ always vanishes. The same condition is obtained for the 1D straight chain of any number N of cells with open and periodic boundaries, which can be shown by applying the Gershgorin circle theorem to the corresponding stability matrix.

It should be emphasized that in Eq. (10), the second and third terms contain geometric information in a_{ij}, b_{ij}

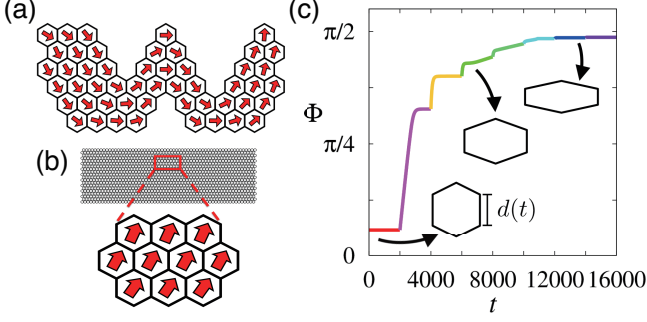


FIG. 4. Polarity pattern for (a) winding cell alignment with a regular hexagonal shape and for (b,c) planar alignment of 60×20 cells with elongated shapes obtained numerically with the phase model [Eqs. (7) and (10)]. In (a), the final pattern is displayed with each arrow indicating the phase of each cell. In (b), phases at $t = 3000$ are displayed. In (c), the time series of the mean phase $\Phi(t)$ defined as $Q(t)e^{i\Phi(t)} = \frac{1}{N} \sum_j e^{i\phi_j(t)}$ with $Q \geq 0$ and $\Phi \in \mathbb{R}$ is displayed. In (b) and (c), cell shape is varied such that the regular hexagon is considered at $t = 0$ and $d(t)$ [indicated in (c)] is decreased by $\frac{\pi}{30}$ at $t = 2000n$ ($n = 1, 2, \dots, 7$), while keeping the perimeter 2π . Initial conditions were chosen such that no topological defects appeared.

and η_{ij} and they facilitate the phase ϕ_i and the mean phase $\frac{\phi_i + \phi_j}{2}$ to be oriented to the cell-to-cell direction η_{ij} , respectively. If only the first term is present in Eq. (10), which is the case in the XY model, there is a family of stable solutions $(\phi_1, \phi_2) = (\phi^*, \phi^*)$ with arbitrary ϕ^* values, and the realized polarity pattern is determined by the initial conditions.

To obtain useful insight into dynamical behavior for a complicated alignment of cells, we further simplify the phase model using the assumption that the neighboring cells are nearly in phase. Under the approximation that $\phi_i = \phi_j$ for any neighboring cells, Eq. (7) with Eq. (10) reduces to

$$\dot{\phi}_i = \epsilon R_i \sin 2(\bar{\eta}_i - \phi_i), \quad (13)$$

where $R_i > 0$ and $\bar{\eta}_i \in \mathbb{R}$ are determined by $R_i e^{i2\bar{\eta}_i} = \sum_{j \in A(i)} (a_{ij} + b_{ij}) e^{i2\eta_{ij}}$, which can be interpreted as the effective strength and the preferred direction of the net interaction of cell i , respectively. We first consider square and hexagonal lattices, where the cell has a square and regular hexagonal shape, respectively. In these cases, R_i vanishes for cell i not facing boundaries of the lattice because a_{ij} and b_{ij} are not i, j -dependent and η_{ij} takes the values $0, 2\pi/n, 4\pi/n, \dots, 2(n-1)\pi/n$ with $n = 4$ and 6 for the square and hexagonal lattices, respectively. On the other hand, for cells at the boundary, R_i is non-vanishing and $\bar{\eta}_i$ is approximately parallel to the boundary line. Therefore, cell polarity at the boundary is oriented parallel to the boundary line and the bulk is smoothly aligned to that of neighboring cells. As shown in Fig. 4(a), this prediction is confirmed using the system with winding cell alignment. In contrast, when the

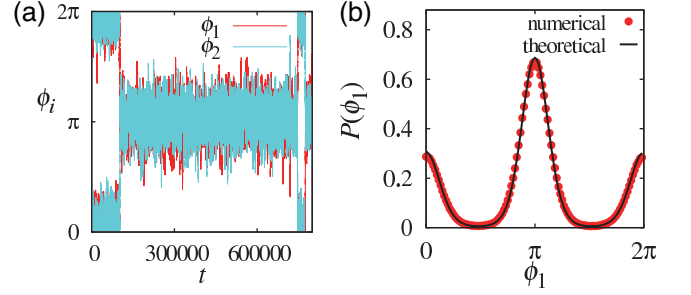


FIG. 5. Polarity orientation in the presence of an external signal and noise in the GLE ($N = 2$). (a) Time series obtained numerically from the reaction-diffusion model [Eq. (1)]. (b) The probability density, where $P(\phi_1) = \int_0^{2\pi} P(\phi_1, \phi_2) d\phi_2$. Numerical results are obtained from direct simulation of Eq. (1) with an inclusion of additive noise $\mathbf{p}_i(\theta_i, t) = (p_i^{(1)}, 0)$ and external signal $\mathbf{G}_i = (\cos(\psi - \theta_i), 0)$ with $\psi = \pi$. (a) Time series. (b) The probability density function obtained numerically and the theoretical one $P(\phi_1) = \int_0^{2\pi} P(\phi_1, \phi_2) d\phi_2$. The parameter values were $\eta_{12} = 0, \nu_1 = 0.005$, and $D_0 = 0.2$ (only for this figure).

cell shape is elongated, R_i is non-vanishing even in the bulk. In this case, $\bar{\eta}_i$ tends to orient to the direction of a contact surface with a larger width. When the number of bulk units is much more than that of boundary units, polarity orientation is dominantly dependent on the cell shape. For example, as shown in Fig. 4(b,c), the polarity tends to be oriented to the direction of the short axis as hexagonal cells are further elongated.

The phase reduction is also possible when our reaction-diffusion model includes external signal and noise (see Supplemental Material B for details). Specifically, we add to Eq. (1) external signal $\epsilon_e \mathbf{G}_i(\theta_i, t)$ and white Gaussian noise $\mathbf{p}_i(\theta_i, t) = (p_i^{(1)}, p_i^{(2)}, \dots)$ that satisfies $E[p_i^{(m)}] = 0$ and $E[p_i^{(m)}(\theta_i, t)p_j^{(n)}(\theta_j, t')] = \nu_m \delta_{ij} \delta_{mn} \delta(\theta_i - \theta_j) \delta(t - t')$ where $E[\cdot]$ denotes the ensemble average and ν_m is the noise intensity. For sufficiently small ϵ_e and ν_m , we obtain

$$\dot{\phi}_i = \epsilon \sum_{j \in A(i)} \Gamma_{ij}(\phi_i, \phi_j) + \epsilon_e \Pi_i(\phi_i) + q_i, \quad (14)$$

where $\Pi_i(\phi_i) = \langle \mathbf{Z}_0(\theta_i - \phi_i), \mathbf{G}_i(\theta_i) \rangle$ and $q_i(t)$ is a white Gaussian noise with zero mean and variance $\nu = \sum_m \nu_m \int_0^{2\pi} Z^{(m)}(\theta)^2 d\theta$ with $Z^{(m)}$ being the m th component of \mathbf{Z} . As a simple example, we consider the GLE with $\mathbf{G}_i = (\cos(\psi - \theta_i), 0)$, where ψ is a parameter, resulting in $\Pi_i = \frac{1}{2\sqrt{1-D_0}} \sin(\psi - \theta_i)$. The phase model under consideration is actually a gradient system, i.e., $\dot{\phi}_i = -\frac{\partial}{\partial \phi_i} \mathcal{H} + q_i$ with the potential function $\mathcal{H} = \mathcal{H}(\{\phi_i\})$ given in Supplemental Material B for details. We thus obtain probability distribution $P(\{\phi_i\}) = C \exp \left[-\frac{2\epsilon \mathcal{H}(\{\phi_i\})}{\nu} \right]$, where C is the normalization constant. As shown in Fig. 5, the probability distribution obtained numerically from the reaction-diffusion model, Eq. (1), is in excellent agreement with $P(\{\phi_i\})$.

Discussion and Conclusion–. A theoretical framework for understanding dynamical properties of alignment process of cellular polarity was proposed. Although the phenomena of our concern are highly nonlinear, our framework enables their analytical treatment even in the presence of noise. Our described framework is readily extendable to treat more concrete problems. For example, the effects of cell heterogeneity and cell shape dependence on local cellular dynamics were examined in previous studies on PCP [6, 8]. These factors can be incorporated into our reaction-diffusion model and the resulting phase model and its dynamical behavior would be of great inter-

est. Overall, we expect that our framework would have many potential applications in nonequilibrium systems including chemical and biological systems.

ACKNOWLEDGMENTS

We are grateful to Dr. Masakazu Akiyama, Dr. Hugues Chate, Dr. Yasuaki Kobayashi, Dr. Yoji Kawamura, Dr. Hiroya Nakao, and Dr. Alexander Mikhailov for helpful discussion and comments. We acknowledge the financial support from CREST, JST and JSPS KAKENHI Grant No. 15K16062.

-
- [1] M. Cross and P. Hohenberg, *Rev. Mod. Phys.* **65**, 851 (1993).
 - [2] H. Meinhardt and A. Gierer, *Bioessays* **22**, 753 (2000).
 - [3] H. Nakao and A. S. Mikhailov, *Nature Physics* **6**, 544 (2010).
 - [4] J. Kosterlitz, *Journal of Physics C: Solid State Physics* **7**, 1046 (1974).
 - [5] D. Devenport, *The Journal of cell biology* **207**, 171 (2014).
 - [6] K. Amonlirdviman, N. A. Khare, D. R. Tree, W.-S. Chen, J. D. Axelrod, and C. J. Tomlin, *Science* **307**, 423 (2005).
 - [7] Y. Burak and B. I. Shraiman, *PLoS Comput Biol* **5**, e1000628 (2009).
 - [8] B. Aigouy, R. Farhadifar, D. B. Staple, A. Sagner, J.-C. Röper, F. Jülicher, and S. Eaton, *Cell* **142**, 773 (2010).
 - [9] T. Ayukawa, M. Akiyama, J. L. Mummery-Widmer, T. Stoeger, J. Sasaki, J. A. Knoblich, H. Senoo, T. Sasaki, and M. Yamazaki, *Cell reports* **8**, 610 (2014).
 - [10] A. Koch and H. Meinhardt, *Reviews of Modern Physics* **66**, 1481 (1994).
 - [11] Y. Kuramoto, *Chemical Oscillations, Waves, and Turbulence* (Springer, New York, 1984).
 - [12] H. Nakao, T. Yanagita, and Y. Kawamura, *Physical Review X* **4**, 021032 (2014).
 - [13] Y. Kawamura and H. Nakao, *Physica D: Nonlinear Phenomena* **295**, 11 (2015).

Supplemental Material for “A Simple Generic Model of Cellular Polarity Alignment: Derivation and Analysis”

K. Sugimura¹ and H. Kori¹

¹*Department of Information Sciences, Ochanomizu University, Tokyo 112-8610, Japan.*

Supplemental Material A: Model equations

Our reaction-diffusion model in the absence of perturbation is given as

$$\frac{\partial}{\partial t} \mathbf{X}_i = \mathbf{F}(\mathbf{X}_i) + \hat{D} \frac{\partial^2 \mathbf{X}_i}{\partial \theta_i^2}. \quad (\text{S1})$$

We consider two exmple models: (a)the real Ginzburg-Landau equation (GLE) and (b)the activator-inhibitor model. With $\mathbf{X}_i = (U_i, V_i)$, the former reads

$$\mathbf{F} = \begin{pmatrix} U_i - (U_i^2 + V_i^2)U_i \\ V_i - (U_i^2 + V_i^2)V_i \end{pmatrix}, \quad (\text{S2})$$

where $\hat{D} = \text{diag}(D_0, D_0)$ and $D_0 = 0.3$. The latter reads

$$\mathbf{F} = \begin{pmatrix} \frac{\rho_U U_i^2}{(1+\kappa U_i^2)V_i} - \mu_U U_i + \sigma_U \\ \rho_V U_i^2 - \mu_V V_i, \end{pmatrix}, \quad (\text{S3})$$

where $\rho_U = 0.01, \rho_V = 0.02, \mu_U = 0.01, \mu_V = 0.02, \sigma_U = 0.0, \kappa = 0.0, \hat{D} = \text{diag}(D_U, D_V), D_U = 0.005, D_V = 0.2$, respectively.

Supplemental Material B: Phase reduction in the presence of external signal and noise

Our reaction-diffusion model in the presense of intercellular interaction, external signal, and noise is given as

$$\frac{\partial}{\partial t} \mathbf{X}_i = \mathbf{F}(\mathbf{X}_i) + \hat{D} \frac{\partial^2}{\partial \theta_i^2} \mathbf{X}_i + \varepsilon \sum_{j \in A(i)} \mathbf{H}_{ij} + \varepsilon_e \mathbf{G}_i + \mathbf{p}_i, \quad (\text{S1})$$

where $\mathbf{G}_i(\theta_i, t)$ is the external signal, ε_e is its strength, and $\mathbf{p}_i = (p_i^{(1)}, p_i^{(2)}, \dots)$ is white Gaussian noise that satisfies $\text{E}[p_i^{(m)}(\theta, t)] = 0$ and $\text{E}[p_i^{(m)}(\theta, t)p_j^{(n)}(\theta', t')] = \nu_m \delta_{ij} \delta_{mn} \delta(\theta - \theta') \delta(t - t')$, and ν_m is the noise intensity. For sufficiently small ε_e and ν_m , we carry on the same procedure as that for Eq. (1) to obtain

$$\dot{\phi}_i = \epsilon \sum_{j \in A(i)} \Gamma_{ij}(\phi_i, \phi_j) + \varepsilon_e \Pi_i(\phi_i, t) + q_i(t) \quad (\text{S2})$$

where

$$\Pi_i(\phi_i) = \langle \mathbf{Z}_0(\theta_i - \phi_i), \mathbf{G}_i(\theta_i, t) \rangle, \quad (\text{S3})$$

$$q_i(t) = \langle \mathbf{Z}_0(\theta_i - \phi_i), \mathbf{p}_i(\theta_i, t) \rangle. \quad (\text{S4})$$

Note that $q_i(t)$ is Gaussian white noise that satisfies $E[q_i(t)] = 0$ and $E[q_i(t)q_j(t')] = \nu\delta_{ij}\delta(t-t')$ with $\nu = \sum_m \nu_m \int_0^{2\pi} d\theta \{Z^{(m)}(\theta)\}^2$ because

$$E[q_i(t)] = E\left[\int_0^{2\pi} d\theta Z(\theta - \phi_i) \cdot \mathbf{p}_i(t) d\theta\right] \quad (\text{S5})$$

$$= E\left[\int_0^{2\pi} d\theta \sum_m Z^{(m)}(\theta - \phi_i) p_i^{(m)} d\theta\right] \quad (\text{S6})$$

$$= \int_0^{2\pi} d\theta \sum_m Z^{(m)}(\theta - \phi_i) E[p_i^{(m)}] d\theta \quad (\text{S7})$$

$$= 0, \quad (\text{S8})$$

and

$$E[q_i(t)q_j(t')] = E\left[\int_0^{2\pi} \int_0^{2\pi} d\theta d\theta' \{ \mathbf{Z}(\theta - \phi_i(t)) \cdot \mathbf{p}_i(t) \} \{ \mathbf{Z}(\theta' - \phi_j(t')) \cdot \mathbf{p}_j(t') \} \right] \quad (\text{S9})$$

$$= E\left[\int_0^{2\pi} \int_0^{2\pi} d\theta d\theta' \left\{ \sum_m Z^{(m)}(\theta - \phi_i(t)) p_i^{(m)}(t) \right\} \left\{ \sum_{m'} Z^{(m')}(\theta' - \phi_j(t')) p_j^{(m')}(t') \right\} \right] \quad (\text{S10})$$

$$= E\left[\int_0^{2\pi} \int_0^{2\pi} d\theta d\theta' \sum_{m,m'} Z^{(m)}(\theta - \phi_i(t)) p_i^{(m)} Z^{(m')}(\theta' - \phi_j(t')) p_j^{(m')}(t') \right] \quad (\text{S11})$$

$$= \int_0^{2\pi} \int_0^{2\pi} d\theta d\theta' \sum_{m,m'} Z^{(m)}(\theta - \phi_i(t)) Z^{(m')}(\theta' - \phi_j(t')) E[p_i^{(m)}(t) p_j^{(m')}(t')] \quad (\text{S12})$$

$$= \int_0^{2\pi} \int_0^{2\pi} d\theta d\theta' \sum_{m,m'} Z^{(m)}(\theta - \phi_i(t)) Z^{(m')}(\theta' - \phi_j(t')) \nu_m \delta_{ij} \delta_{mm'} \delta(\theta - \theta') \delta(t - t') \quad (\text{S13})$$

$$= \int_0^{2\pi} d\theta \sum_m \nu_m \left\{ Z^{(m)}(\theta - \phi_i(t)) \right\}^2 \quad (\text{S14})$$

$$= \sum_m \nu_m \int_0^{2\pi} d\theta \left\{ Z^{(m)}(\theta) \right\}^2. \quad (\text{S15})$$

In the case of GLE, any generic choice of external signal $\mathbf{G}_i(\theta_i, t)$ yields

$$\Pi_i = c_i(t) \sin(\psi_i(t) - \theta_i) \quad (\text{S16})$$

because $\mathbf{Z}_0(\theta)$ contains only the first harmonics. As a simple example, we consider

$$\mathbf{G}_i(\theta_i) = (\cos(\psi(t) - \theta_i), 0), \quad (\text{S17})$$

where $\psi_i(t)$ is a parameter, we obtain

$$\Pi_i = \frac{1}{2\sqrt{1-D_0}} \sin(\psi - \theta_i). \quad (\text{S18})$$